# Nitrogen-related point defects in homoepitaxial diamond (100) freestanding single crystals

T. Teraji[1,*], C. Shinei[1]

[1] *Research Center for Functional Materials, National Institute for Materials Science, 1-1 Namiki, Tsukuba, Ibaraki 305-0044, Japan*

Abstract

Controllability of nitrogen doping, types of nitrogen-related defects, and their charge states in homoepitaxial diamond (001) crystals were investigated. For these purposes, $^{15}$N-doped $^{12}$C-enriched free-standing chemical vapor deposited (CVD) diamond (001) crystals were grown through long-time growth using $^{12}$C-enriched methane as the carbon source gas and $^{15}$N-enriched molecular nitrogen as the nitrogen source gas. Formation of non-epitaxial crystallites and growth hillocks was suppressed by application of the oxygen-adding growth condition. Nitrogen was incorporated uniformly into the crystals, with concentration variation of less than 10%. About 70% of the total nitrogen was substitutional nitrogen in a neutral charge state $N_s^0$. Hydrogen was incorporated at approximately the same concentration as nitrogen. Both NV and NVH centers were predominantly negatively charged defect structures, i.e., $NV^-$ and $NHV^-$ centers. The concentrations of $NHV^-$ centers were less than 5% of the total nitrogen concentration. Nitrogen concentration in diamond crystals was controlled by changing the N/C gas ratio over a wide doping range from 10 ppb to 10 ppm. Nitrogen incorporation efficiency was found to be $(1.5\pm0.5) \times 10^{-4}$ in this study.

Key words: $^{12}$C; chemical vapor deposition; diamond; hydrogen; $^{15}$N; nitrogen

*Corresponding author. Tel: +81-29-860-4776. E-mail: TERAJI.Tokuyuki@nims.go.jp (Tokuyuki Teraji)

## 1. Introduction

Research to elucidate weak magnetic field detection using NV centers in diamond has been pursued intensively world-wide. The minimum detectable magnetic field is defined by shot noise.[1] That equation indicates to us that the sensitivity becomes higher when one increases both the concentration of $NV^-$ centers and the coherence time of electron spins $T_2$. Dense $NV^-$ centers are often created by forming vacancies in nitrogen-doped diamond crystals using electron-beam irradiation followed by high-temperature annealing. Here, nitrogen doping in diamond crystal is the first step to controlling the concentration of NV centers. To date, diamond crystals with $NV^-$ center concentrations [$NV^-$] of 0.4–3.8 ppm have been used for weak magnetic field detection.[2, 3, 4, 5] The nitrogen concentration [N] (or substitutional nitrogen concentration [$N_s$]) of these diamond crystals is in the range of 1.4–28 ppm, which is approximately 5–10 times that of [$NV^-$]. Shinei *et al.* reported that the NV centers are predominantly negatively charged (i.e., $NV^-$ centers) when the ratio of [$NV^-$] to [$N_s$] is below 10%.[6] Considering these reported findings, target [N] for the weak magnetic field detection is 1–30 ppm. Controlling the nitrogen concentration [N] in the diamond crystal within this concentration range is crucially important for increasing magnetic sensing sensitivity.

In addition to limiting the nitrogen concentration to this doping range, increasing the coherence time is important to improve the magnetic sensitivity. Diamond is generally composed of 98.9% $^{12}C$ with no nuclear spin and 1.1% $^{13}C$ with a nuclear spin $S$=1/2. Elimination of the nuclear spins attributed to $^{13}C$ is necessary to increase the coherence time of the electron spins of the $NV^-$ centers.[7] Consequently, carbon isotopic enrichment of diamond crystal with $^{12}C$ carbon is a key task for quantum sensor application. Additionally, impurities that cause decoherence must be minimized.

Two representative diamond growth methods, high-temperature and high-pressure (HPHT) synthesis method and chemical vapor deposition (CVD) method, entail benefits and shortcomings for these requirements described above. During the HPHT method, approximately 100 ppm of nitrogen is naturally incorporated in the diamond crystals. Therefore, higher doping of nitrogen is easy. Using this method, the nitrogen concentration in diamond can be controlled at the parts per million level by adjusting the weight percentage of nitrogen-gettering metal solvents such as titanium.[8] During diamond growth by the HPHT method, impurities are incorporated from the air, metal solvents and components of the reaction cell. Therefore, it is generally difficult to obtain crystals with high chemical purity and high isotope enrichment when using the HPHT method. Reportedly, HPHT crystals have a $^{12}C$ enrichment of 99.995% when polycrystalline diamond with $^{12}C$ enrichment of 99.998% is used as the carbon source material.

The microwave-plasma CVD growth method is superior to the HPHT synthesis method in terms of increasing both the chemical purity and isotope enrichment of diamond crystals.[9, 10, 11] Nitrogen addition during diamond CVD growth is frequently undertaken to enhance the diamond growth rate.[12] This nitrogen addition increases the diamond growth rate by approximately 2–2.5 times.[13, 14, 15] However, the difficulty achieving high-concentration nitrogen doping when using the CVD method has been pointed out.[16] Molecular nitrogen is commonly used as a nitrogen dopant for CVD diamond growth. Nitrogen incorporation efficiencies during diamond growth reportedly range from $3 \times 10^{-5}$ to $7 \times 10^{-2}$ when using molecular nitrogen.[14, 15, 16, 17] Here, the nitrogen incorporation efficiency is defined as the ratio of incorporated nitrogen in diamond crystal to the gas ratio of the nitrogen gas flow rate to the methane gas flow rate (N/C gas ratio) during CVD growth. This impurity incorporation efficiency is low compared to boron incorporation of approximately 1 or more.[18] Because of this low efficiency of nitrogen incorporation, the N/C gas ratio of over 10–30,000 ppm must obtain diamond with the substitution nitrogen concentration [$N_s$] of 1 ppm.

When nitrogen is introduced as a reactive gas at a high concentration, reactive species and reaction processes that contribute to diamond growth are expected to be influenced and altered. The low and highly variable nitrogen incorporation efficiencies, ranging from $3 \times 10^{-5}$ to $7 \times 10^{-2}$, and depending on the growth conditions, might be a primary factor in reducing the reproducibility of diamond CVD growth experiments. Therefore, stable growth conditions are necessary for the precise control of the nitrogen concentration.

Regarding the change of crystalline quality by nitrogen doping, the diamond crystal quality reportedly deteriorates when [$N_s$] exceeds 4 ppm.[19] However, Mokuno *et al.* succeeded in growing a CVD diamond plate with a low dislocation density of 400 $cm^{-2}$ using high-quality HPHT type IIa(001) diamond crystal as a substrate. Here, the CVD diamond plate was doped intentionally with nitrogen so that [$N_s$] became 1 ppm.[20] These reported findings indicate that the relation between [$N_s$] and crystal quality is not sufficiently understood. Tallaire *et al.* reported that the nitrogen incorporation efficiency became a larger value of $5 \times 10^{-2}$ and that defect generation was well suppressed when using $N_2O$ gas as a nitrogen dopant instead of nitrogen molecules.[16, 21] The nitrogen incorporation efficiency is higher, presumably because of the dissociation of large amounts of $N_2O$ gas in the plasma.

We have reported that the crystalline quality of diamond is improved by adding 2% oxygen during diamond CVD growth.[9] The application of oxygen-adding diamond growth conditions to high-nitrogen-concentration diamond growth can be expected to improve both the crystalline quality of nitrogen-doped diamond and the controllability of nitrogen concentration in the diamond crystal. From this perspective, it can be understood that oxygen atoms contained in $N_2O$ gas are effective at improving the quality of nitrogen-doped CVD diamond crystals.[14, 21] These facts suggest that the

degradation of diamond crystal quality caused by nitrogen doping with [$N_s$] at concentrations higher than 1 ppm can be minimized by the application of oxygen-adding growth conditions. Furthermore, when using molecular nitrogen, nitrogen isotope enrichment becomes possible because, for example, $^{15}N$ nitrogen molecular gas is commercially available.

For this study, nitrogen-doped free-standing crystals with 0.3 mm or greater thickness were grown using MPCVD method. Then the types and concentrations of nitrogen-related defects formed in the crystals were evaluated. To suppress the deterioration of crystallinity caused by nitrogen doping, the growth conditions of oxygen addition were applied. Molecular nitrogen gas including $^{15}N$ enriched gas ($^{15}N_2$) was used to grow nitrogen-doped diamond crystals. Diamond growth by $^{12}C$ enrichment was performed simultaneously. Results show that the nitrogen incorporation efficiency (the ratio of nitrogen concentration in the diamond crystal to the N/C ratio of the gas flow rate) is constant over a range of nitrogen concentrations extending over three orders of magnitude when nitrogen molecular gas is used as a dopant and oxygen addition conditions are applied for diamond CVD growth.

## 2. Experiments

Homoepitaxial diamond films were grown using the microwave-plasma CVD system developed at the National Institute for Materials Science (NIMS). Details of the microwave-plasma CVD system are described elsewhere.[10, 22] For this study, $^{12}C$ isotopically enriched methane for which the enrichment was specified to >99.9% was used as a carbon source gas. Chemical purity specifications of source gases are 9N for hydrogen (using a palladium purifier), 8N for methane (using a zirconium purifier), and 6N5 for oxygen.

For homoepitaxial film growth, HPHT-grown type-Ib (100) substrates with dimensions of 3.5 × 3.5 $mm^2$ in area and 1-mm thickness were used. Then $^{15}N_2$ gas (chemical purity >3N), for which the enrichment was specified to 98%, was used as a nitrogen doping gas for samples. The CVD conditions included the following: 110 Torr reaction pressure, 1.4 kW microwave power, 10% methane concentration ratio (flow rate ratio of $CH_4$ to the total gas flow), 2% oxygen concentration (flow rate ratio of $O_2$ to the total gas flow), and 1020–1090°C substrate temperature. A disappearing filament optical pyrometer (DFP 2000; Spectrodyne Inc.) was used for temperature measurements of the diamond sample during CVD growth. As an exception, sample 4 was grown with 1.7 kW microwave power and nitrogen gas (chemical purity >6N5, natural abundance isotope ratio). The N/C gas ratios during diamond growth and the dimensions of the respective samples are presented in Table I.

Microscopic images of free-standing CVD diamond plate were obtained using a stereomicroscope (SZ61; Olympus Corp.). Impurities in the diamond crystals were characterized

using secondary ion mass spectrometry (SIMS, IMS-7f, CAMECA; Ametek Inc.), Fourier transform infrared spectroscopy (FTIR, FT/IR-6600; Jasco Corp.), electron paramagnetic resonance (EPR, JES-FA100; JEOL Ltd.), and photoluminescence (PL, Nanofinder FLEX; Tokyo Instruments, Inc.) methods. The $^{12}C$ isotope enrichment of homoepitaxial diamond films was evaluated based on SIMS measurements.

## 3. Results and Discussion

### 3.1 Optical microscope image

Figure 1(a) portrays a microscopic image of the as-grown state of sample 1 taken in the brightfield reflection mode. The $^{15}N/C$ ratio in the gas phase applied for the diamond growth of sample 1 was 20,000 ppm. The CVD layer thickness was 430 μm. A feature of step bunching was observed on the surface of the as-grown homoepitaxial film.[23] Because defect formation was suppressed by the addition of oxygen, non-epitaxial crystallites and growth hillocks did not form on the sample surface even after a long period of growth. The blue dashed rectangle corresponds to the substrate position. Polycrystalline diamond was partially grown at the rim of the substrate. To create free-standing CVD diamond (001) crystals, the top surface of the sample was first laser-cut into a square shape to cut out the polycrystalline diamond portion. Then the sample was laser-cut from the side to remove the CVD layer from the substrate. Figures 1(b) and 1(c) respectively depict microscopic images of free-standing shaped sample 1 taken in the brightfield reflection mode and birefringence image mode. The color of sample 1 after being processed into a free-standing plate is transparent, as shown in Fig. 1(b). A four-fold symmetric

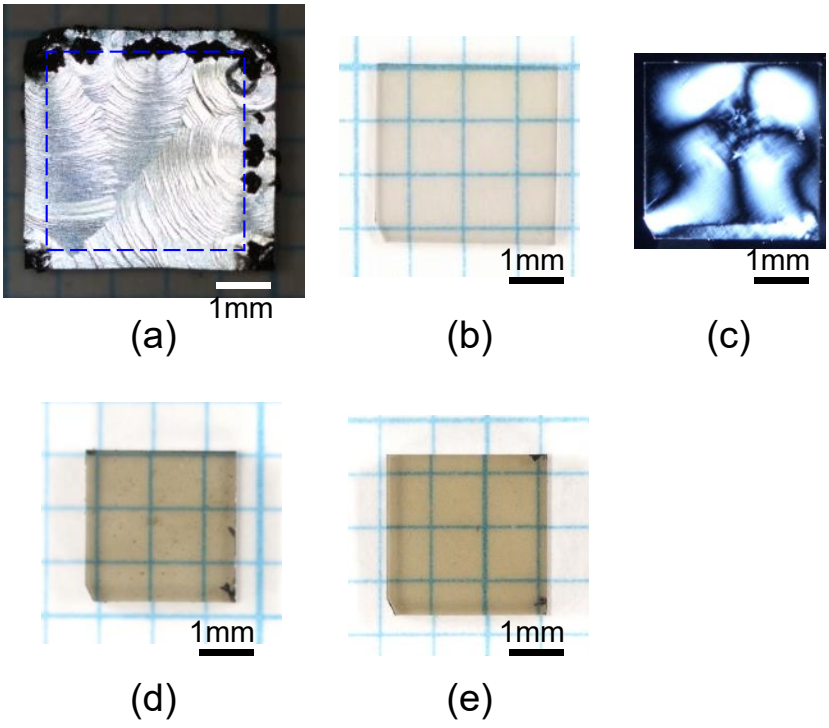


Figure 1 Optical microscope images of homoepitaxial diamond crystals. Brightfield reflection images of sample 1 (a) in an as-grown state and (b) after removal from the substrate. (c) Birefringence image of sample 1 after removal from the substrate. Brightfield reflection images of (d) sample 2 and (e) sample 3 after removal from the substrate.

Table I. N/C gas ratios applied for diamond growth of samples 1–5 and sample dimensions for each sample

| | Sample 1 | Sample 2 | Sample 3 | Sample 4 | Sample 5 |
|---|---|---|---|---|---|
| N/C gas ratio [ppm] | 20,000 | 40,000 | 80,000 | 0 | 40,000 |
| Area [$mm^2$] | 3.3 × 3.3 | 2.8 × 2.8 | 2.9 × 2.9 | 3.0 × 3.0 | 3.0 × 3.0 |
| Thickness [mm] | 0.3 | 0.5 | 0.9 | 0.3 | 1.2 |

pattern was observed in the birefringence image, as shown in Fig. 1(c). This symmetrical feature, reflecting the {111} growth sector in high-temperature-high-pressure synthesis, is commonly observed in birefringence images of commercially available HPHT-grown type-Ib(001) substrates. High-density dislocations in the center of the sample also reflect the dislocation distribution of the substrate, indicating that the strain of the free-standing plate is induced from the substrate and that the crystal strain can be minimized using a low-strain substrate.

Figures 1(d) and 1(e) show microscopic images taken in the bright field reflection mode for samples 2 and 3. The $^{15}N/C$ ratio in gas phase applied for diamond growth of samples 2 and 3 were, respectively, 40,000 ppm and 80,000 ppm. These images show their color as light brownish, as commonly observed from nitrogen-doped CVD diamond plates.[24] This brownish color might be attributable to the creation of vacancy clusters.[25]

### 3.2 SIMS characterization

Figures 2(a)–2(c) portray depth profiles of the impurities in samples 1–3, as measured using SIMS. Again, these samples were grown with $^{12}C$ enriched methane and $^{15}N$ enriched nitrogen. The respective $^{15}N/C$ ratios in gas phase are 20,000, 40,000, and 80,000 ppm. $^{15}N$ was detected clearly from these samples by SIMS measurements. $^{14}N$ and boron were not detected in these diamond samples. In Fig. 2, with elements for which the detected signal is below the background level, a plateau region is apparent in the signal. This plateau configuration does not reflect the actual concentration of the element. It is an artifact because of the detection limit of the detector. Large amounts of hydrogen were detected from these three samples. The depth profile of hydrogen resembles that of $^{15}N$. SIMS results reveal the hydrogen concentration as 1.5–4 times higher than that of nitrogen. Sample 4 was grown using the same CVD set-up, but without nitrogen feeding. Nitrogen, hydrogen, boron, and silicon for sample 4 were below the detection limit.

Sample 5 is grown with nitrogen in natural abundance, which comprises 99.636% $^{14}$N and 0.364% $^{15}$N. Also, $^{14}$N was detected clearly from this sample. Sample 6 was prepared to assess the concentration of $^{12}$C of the CVD diamond crystals grown for this study. This sample was first grown using the $^{12}$C-enriched methane. The $^{12}$C diamond film thickness was about 250 nm. A diamond film was then grown using methane with natural abundance (NA) of carbon on the $^{12}$C-enriched

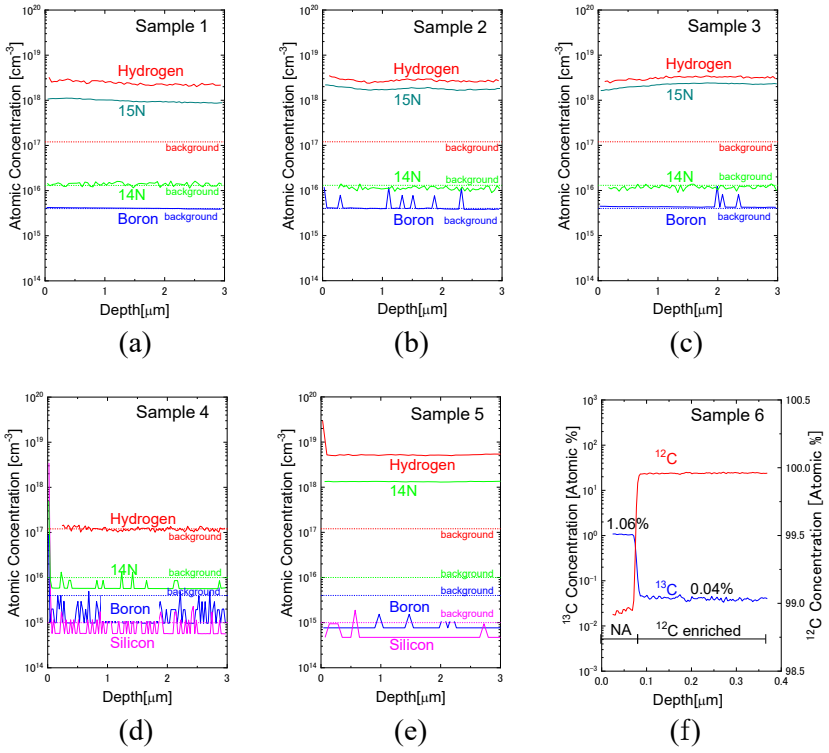


Figure 2 Nitrogen, hydrogen, and boron depth profiles of (a) sample 1, (b) sample 2, (c) sample 3, (d) sample 4, and (e) sample 5. Silicon depth profiles are also shown for samples 4 and 5. (f) $^{12}$C and $^{13}$C depth profiles of sample 6.

Table II. N/C gas ratios applied for diamond growth of samples 1–5 and nitrogen concentration of each sample measured by SIMS. SD and DL in the list respectively denote the standard deviation and detection limit

| | Sample 1 | Sample 2 | Sample 3 | Sample 4 | Sample 5 |
|---|---|---|---|---|---|
| N/C gas ratio [ppm] | 20,000 | 40,000 | 80,000 | 0 | 40,000 |
| [N] average [ppm] | 5.539 | 10.26 | 12.46 | DL | 7.56 |
| [N] SD [ppm] | 0.45 | 0.69 | 1.23 | DL | 0.09 |
| Incorporation Eff. | 2.8.E-04 | 2.6.E-04 | 1.6.E-04 | | 1.9.E-04 |
| [H] average [ppm] | 13.6 | 15.6 | 0.0 | DL | 29.5 |
| [H] SD [ppm] | 1.3 | 1.2 | 1.4 | DL | 0.7 |

diamond film. The film thickness of diamond of NA carbon was 70 nm. The $^{13}$C atomic concentration in the diamond film grown in natural abundance methane shows good agreement with the well-known

natural abundance value of carbon, indicating that $^{13}C$ can be assessed adequately using SIMS. The SIMS results reveal the concentration of $^{12}C$ of the samples examined for this study as 99.96%.

The average value and standard deviation (SD) of $^{15}N$ for samples 1–5 are presented in Table I. The unit of concentration is parts per million. Nitrogen concentration [N] increases with increasing N/C ratio in the gas phase. The standard deviation of nitrogen concentration is below 1/10 of the [N] average, meaning that nitrogen is incorporated homogeneously into diamond crystal.

Comparison of the nitrogen [N] and hydrogen [H] concentrations of sample 2 and sample 5 grown at the sample N/C gas ratio of 40,000 ppm shows that the [N] and [H] of sample 5 are, respectively, 74% and 189% of those found for sample 2. This fact suggests that the incorporation efficiencies of hydrogen and nitrogen are inversely correlated. Regarding growth conditions, a difference was found in the substrate temperature during CVD growth; the growth temperatures were 1020–1050°C for sample 2 and 1070–1090°C for sample 5, with the temperature about 50°C higher for sample 5. This finding suggests that more hydrogen is incorporated at higher temperatures. However, another sample was found to have an N/C gas ratio of 50,000 ppm, which is more than that of sample 2. A similar growth temperature to that of sample 2 had less [H] than sample 2. At this time, it remains unknown what growth parameters aside from the nitrogen concentration in gas phase affect hydrogen incorporation. Additional systematic experiments must be conducted.

### 3.3 EPR characterization

Figures 3(a)–3(c) show spectra obtained using electron paramagnetic resonance (EPR) spectroscopy for samples 1–3. Because field modulation and lock-in detection were used, the EPR spectra were obtained in terms of derivative absorption. The P1 center, which is neutrally charged substitutional nitrogen and the same as $N_s^0$, was detected from these

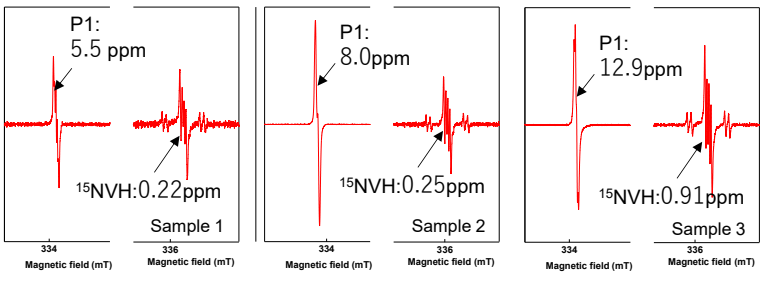


(a) (b) (c)

Figure 3 EPR spectra of (a) sample 1, (b) sample 2, and (c) sample 3. Signals corresponding to the P1 center and $^{15}NVH$ center are shown.

Table III. N/C gas ratios applied for diamond growth of samples 1–3 and concentration of nitrogen related impurities of each sample measured using EPR

| | Sample 1 | Sample 2 | Sample 3 |
|---|---|---|---|
| N/C gas ratio [ppm] | 20,000 | 40,000 | 80,000 |
| P1 ($N_s^0$) [ppm] | 5.5 | 8.0 | 12.9 |
| $NVH^-$ [ppm] | 0.22 | 0.25 | 0.91 |

samples, as shown in in the left panel of Figs. 3(a)–3(c). These EPR spectra show half of the EPR spectra, corresponding to an overlap of the four hyperfine peaks which originate from the four symmetry-related sites of $^{15}N_s$. The signal intensity of the P1 center increased with increasing $^{15}N/C$ ratio in the gas phase. The $NVH^-$ center with $^{15}N$ was also detected, as shown in the right panel of Figs. 3(a)–3(c). Because we used $^{15}N_2$ as the nitrogen source gas, the resonance frequency of the $NVH^-$ centers did not overlap with that of the P1 centers, which allowed accurate estimation of the concentration of the $NVH^-$ centers.[26] A hydrogen hyperfine structure was observed at the foot of the $NVH^-$ center. The signal of the $NV^-$ center from these samples was too small to detect using EPR. This finding is consistent with the reported fact that the concentration of $NV^-$ center is about 1/100-fold lower than that of P1 centers.[14] The relevant EPR data for samples 1–3 are presented in Table III.

The P1 concentration [P1] was comparable to the nitrogen concentration [N] obtained from SIMS measurements. This finding indicates that most of the nitrogen is incorporated into the diamond crystal as neutrally charged substitutional nitrogen. The concentration of $NVH^-$ centers is 5–10% of that of P1 centers. This result is consistent with those reported from earlier studies.[14, 27, 28, 29] As Table II shows, SIMS measurements detected hydrogen in nitrogen-doped CVD diamonds at concentrations 1.5–4 times higher than that of nitrogen. It is apparent that the ratio of NVH is small with respect to the total amount of hydrogen incorporated in the nitrogen-doped CVD diamonds.

### 3.4 FTIR characterization

Figures 4(a)–4(i) portray spectra obtained using Fourier transform infrared (FTIR) spectroscopy. Measurements were taken with the sample placed in a nitrogen atmosphere. When the nitrogen concentration is as high as 25 ppm or more, the $N_s^0$ absorption peak appears at 1130 $cm^{-1}$. [30] A coefficient for converting absorption intensity at 1130 $cm^{-1}$ to $[N_s^0]$ is reportedly 25± 2 ppm cm. The 1130 $cm^{-1}$ peak shifts to 1121 $cm^{-1}$ when replacing $^{14}N$ with $^{15}N$. [31] When the nitrogen concentration is lower, the peak at 1121 $cm^{-1}$ becomes too small to detect.

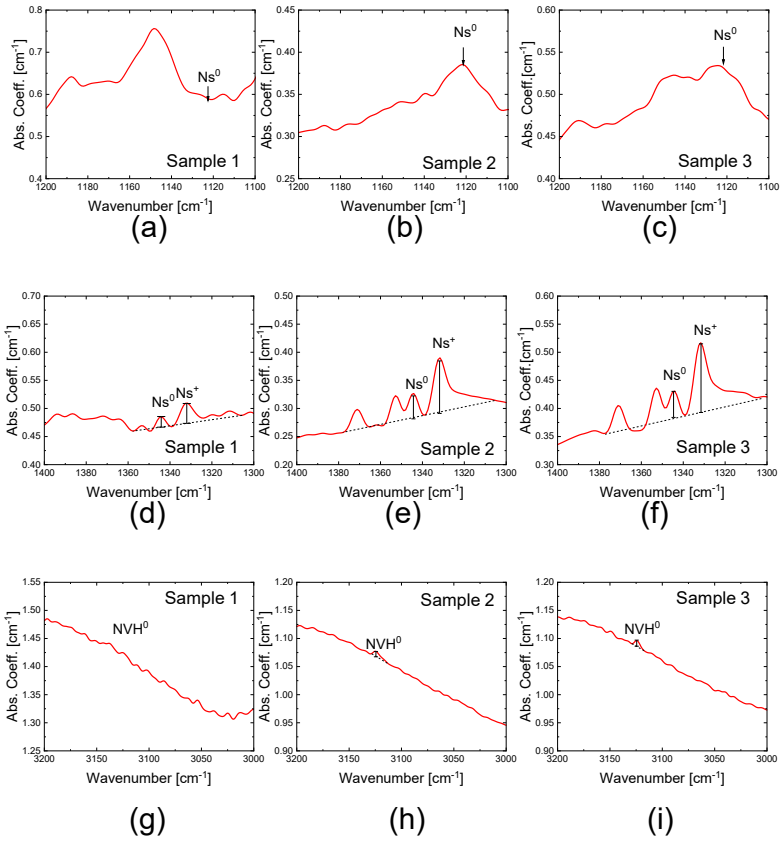


Figure 4 FTIR absorption spectra corresponding to (a)–(c) $N_s^0$, (d)–(f) $N_s^+$, and (g)–(h) $NVH^0$ centers. The FTIR spectra of sample 1 are (a), (d), and (g), those of sample 2 are (b), (e), and (h), and those of sample 3 are (c), (f), and (i).

Another detection method proposed by Lawson *et al.* was used to estimate $[N_s^0]$ using the absorption peak for samples with lower nitrogen concentration.[30] This method uses the absorption peak at 1344 $cm^{-1}$ to estimate $[N_s^0]$ instead of the absorption peak at 1130 $cm^{-1}$ (or 1121 $cm^{-1}$ for $^{15}N$). By comparing the absorption intensity of the FTIR spectrum of the same sample with the [P1] value obtained using the EPR measurement as the reference value, a coefficient for converting absorption intensity at 1344 $cm^{-1}$ to $[N_s^0]$ was determined to be 261,000 ppm cm. This coefficient value was used for this study to estimate $[N_s^0]$. As described above, $N_s^0$ is called the P1 center for EPR measurements.

The concentration of $N_s^+$ was estimated from the absorption peak at 1332 $cm^{-1}$.[30] The coefficient for converting absorption intensity at 1332 $cm^{-1}$ to $[N_s^+]$ was found to be 38,800. This value was obtained as follows. The coefficients for converting absorption intensity at 1344 $cm^{-1}$ to $[N_s^0]$ and at 1332 $cm^{-1}$ to $[N_s^+]$ are reported respectively as 37,000 ppm cm and 5500 ppm cm.[30] A coefficient ratio for $[N_s^+]$ to $[N_s^0]$ is 0.149. By multiplying 0.149 with 261,000 ppm cm, which is the coefficient

for [$N_s^0$] found from this study, the coefficient for [$N_s^+$] was obtained as 38,800 ppm cm. The estimated values of [$N_s^0$] and [$N_s^+$] are presented in Table IV.

The difference in [$N_s^0$] values estimated from the absorption intensities at 1344 $cm^{-1}$ and 1121 $cm^{-1}$ is less than 20%. The absorption intensity at 1121 $cm^{-1}$ was too small to be detected for sample 1. In the following, [$N_s^0$] values estimated from the absorption intensities at 1344 $cm^{-1}$ were used for analysis. The absorption intensity of both [$N_s^0$] and [$N_s^+$] becomes larger with increase of the $^{15}N/C$ ratio in gas phase. The fraction of $N_s^0$ to total substitutional nitrogen, [$N_s^0$]/([$N_s^0$]+[$N_s^+$]), is higher than three, indicating that the substitutional nitrogen is predominantly in a neutral charge state. This result is consistent with the discussion presented in subsection 3.3: the nitrogen incorporated in the CVD diamond crystals has a mostly neutrally charged state. Substitutional nitrogen in a neutral charge state is suitable for the formation of $NV^-$ centers because $N_s^0$ becomes the donor which provides the negative charge to form the $NV^-$ center.

Table IV. N/C gas ratios applied for diamond growth of samples 1–3 and concentration of nitrogen related impurities of each sample measured using FTIR. In the table, $N_s^0$ estimated from absorption at 1344 $cm^{-1}$ was used for obtaining $N_s^0/(N_s^0+N_s^+)$. DL in the list denotes the detection limit.

| | Sample 1 | Sample 2 | Sample 3 |
|---|---|---|---|
| N/C gas ratio [ppm] | 20,000 | 40,000 | 80,000 |
| $N_s^0$ [ppm] (1121 $cm^{-1}$) | DL | 9.5 | 13.0 |
| $N_s^0$ [ppm] (1344 $cm^{-1}$) | 4.9 | 11.1 | 12.9 |
| $N_s^+$ [ppm] (1332 $cm^{-1}$) | 1.37 | 3.78 | 4.89 |
| $N_s^0/(N_s^0+N_s^+)$ | 78% | 75% | 73% |
| $NVH^0$ [ppm] | DL | 0.01 | 0.01 |

Absorption at 3123 $cm^{-1}$ is attributed to the $NVH^0$ center.[32] As shown in Figs. 3(g) and 3(i), the absorption intensity of the $NVH^0$ center of samples 2 and 3 was detected, but that of sample 1 was too small to be detected. Concentrations of the $NVH^0$ center estimated using the reported calibration coefficient[33] of 0.2 ppm $cm^2$ are approximately 0.01 ppm for both samples 2 and 3. Comparison of these with [$NVH^-$] values obtained from EPR measurements shows that the concentration ratio of [$NVH^0$] to [$NVH^-$] is less than 0.1. The predominance of the negatively charged $NVH^-$ center might derive from the abundant presence of donor $N_s^0$ in the diamond crystal, as discussed above.

### 3.5 PL characterization

Figure 5(a) portrays the photoluminescence (PL) spectra of samples 1–3. The zero-phonon line (ZPL) of $NV^-$ center is 637 nm. That of the $NV^0$ center is 575 nm. The emission band in the wavelength range of 640–720 nm is the phonon sideband of the $NV^-$ center, whereas the emission band in the wavelength range of 580–670 nm is the phonon sideband of the $NV^0$ center.[34] Total intensity of NV-center related luminescence increased with the $^{15}N/C$ ratio in gas phase. The luminescence intensity of ZPL of $NV^-$ center ($I_{ZPL}(NV^-)$) was stronger than that of ZPL of $NV^0$ center ($I_{ZPL}(NV^0)$), which means that most of the NV center is negatively charged. Table V presents $I_{ZPL}(NV^-)$, $I_{ZPL}(NV^0)$, $[NV^0]/[NV^-]$, and $[NV^-]/[NV_{Total}]$. Here, to estimate the concentration ratio, we used the Huang–Rhys factor and PL lifetime.[6]

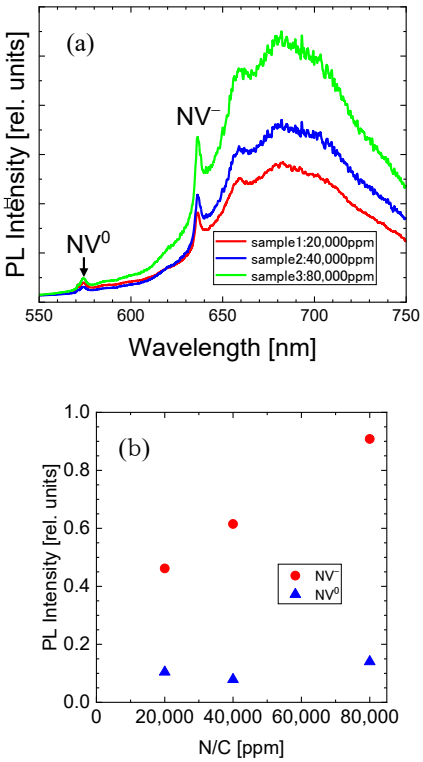


Figure 5 (a) PL spectra of samples 1–3. (b) Zero-phone line of the $NV^-$ and $NV^0$ centers of samples 1–3.

Figure 5(b) shows $I_{ZPL}(NV^-)$ and $I_{ZPL}(NV^0)$ as a function of the $^{15}N/C$ ratio in the gas phase. It is apparent that $I_{ZPL}(NV^-)$ increases monotonically with the $^{15}N/C$ gas ratio, whereas $I_{ZPL}(NV^0)$ is constant. The concentration ratios $[NV^0]/[NV^-]$ of samples 1–3 are, respectively, 0.19, 0.11 and 0.13. We also estimated the ratio of $[NV^-]$ to the total amount of NV center $[NV_{Total}]$, which is the sum of $[NV^-]$ and $[NV^0]$, as shown in the last row of Table V. It shows that approximately 90% of

Table V. N/C gas ratios applied for diamond growth of samples 1–3 and the concentration ratios of $NV^0$ to $NV^-$ of samples measured using PL

| | Sample 1 | Sample 2 | Sample 3 |
|---|---|---|---|
| N/C gas ratio [ppm] | 20,000 | 40,000 | 80,000 |
| I_($NV^-$) [rel. units] | 2,770 | 3,690 | 5,450 |
| I_($NV^0$) [rel. units] | 626 | 472 | 842 |
| $[NV^0]/[NV^-]$ | 0.19 | 0.11 | 0.13 |
| $[NV^-]/[NV_{Total}]$ | 0.84 | 0.90 | 0.89 |

the NV centers are in a negatively charged state. For as-grown CVD diamond, the ratio of [$NV_{Total}$] to [$N_s^0$] is typically smaller than 0.1.[27, 29] This small value of [$NV_{Total}$]/[$N_s^0$] ratio of <0.1 is likely to be the reason for the high [$NV^-$]/[$NV_{Total}$] value of approximately 0.9.[6, 35]

### 3.6 Abundance ratio of nitrogen-related defects

Based on the measurement results presented above, the abundance ratio of each nitrogen-related defect was evaluated, as depicted in Fig. 6. More than 95% of nitrogen is located as substitutional nitrogen. About 70% of the nitrogen is $N_s^0$; 20–30% of the nitrogen is $N_s^+$. Nitrogen below 5% was in the $NVH^-$ centers. Although the total amount of nitrogen varies from 5 ppm to 12 ppm among samples 1–3, no apparent differences exist in the abundance ratios of nitrogen-related defects.

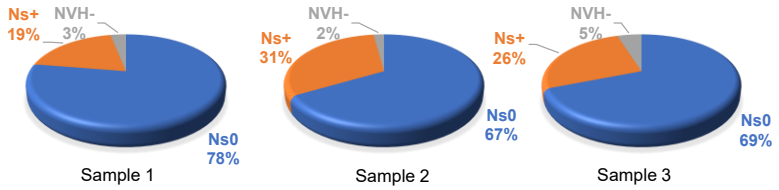


Figure 6 Abundance ratios of nitrogen-related defects of samples 1–3.

[$N_s^+$] is reported as negligibly small compared to [$N_s^0$] in HPHT type Ib diamonds with a total nitrogen concentration of 9 ppm.[30] The presence of $N_s^+$ at 20–30% of the total nitrogen content implies the presence of acceptors in CVD diamond crystals at similar concentrations to nitrogen. Although boron is a typical acceptor for diamond, its concentration in the CVD diamond investigated for this study is below the detection limit of SIMS measurement, 0.2 ppm, as shown in Fig. 2. The fundamental difference between nitrogen-doped CVD diamond and nitrogen-doped HPHT diamond is that hydrogen is present in the crystal in the former, almost in the same amount as nitrogen. However, it remains unknown whether hydrogen has a role as an acceptor in diamond. Further investigation must be undertaken to clarify the origin of acceptors formed in nitrogen-doped CVD diamond.

### 3.7 Control of nitrogen concentration and hydrogen incorporation

Figure 7(a) presents the nitrogen concentration [N] estimated by SIMS (red circles) and [P1] (blue triangles) and measured by EPR, as a function of N/C gas ratio. Nearly equal values of [N] and [P1] indicate that nitrogen is incorporated as $N_s^0$ in the neutrally charged state. These data were aligned on a straight line (a straight line with a slope of 45 degrees on a log-log plot) over three orders of magnitude of nitrogen concentration. Finally, the nitrogen concentration in diamond crystals was controlled successfully from 10 ppb to 10 ppm by changing the N/C gas ratio. The slope of this straight line corresponds to the incorporation efficiency, which is a ratio of $[N_s^0]$ to N/C ratio in the gas phase. The efficiency was estimated as $(1.9\pm0.2) \times 10^{-4}$, which is two orders of magnitude lower than the incorporation efficiency using $N_2O$ as a nitrogen source gas, suggesting a difference of decomposition efficiency of nitrogen-related gas in plasma.

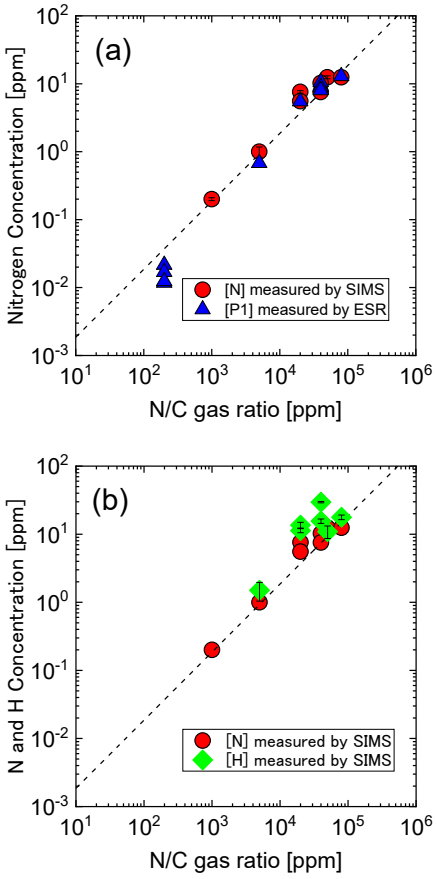


Figure 7 (a) Nitrogen concentrations as estimated by SIMS (red circles) and (blue triangles) and as measured using EPR, as a function of the N/C gas ratio. (b) Hydrogen concentrations (green diamonds) estimated using SIMS as a function of the N/C gas ratio, along with the nitrogen concentration.

Figure 7(b) shows the hydrogen concentration [H] (green diamonds) estimated using SIMS as a function of the N/C gas ratio, along with the nitrogen concentration. It is apparent that the hydrogen concentration is roughly proportional to the nitrogen concentration. As SIMS revealed, the hydrogen and nitrogen depth profiles are correlated. Moreover, hydrogen was below the SIMS detection limit (approx. 0.5 ppm) for the non-doped sample. These findings suggest that hydrogen is incorporated in a form bonded to nitrogen. At least, the hydrogen incorporation in diamond crystals is induced by nitrogen doping.

The reproducibility of impurity concentrations during sample growth is also apparent from Fig. 7. First, in Figs. 7(a) and 7(b), there is about 10% variation in the depth direction of each sample, as indicated by the error bars in the figures. Second, the variation among multiple samples grown under identical conditions can be understood from variation in the data plot in Fig. 7. For example, when grown at N/C=40,000 ppm, the nitrogen concentration was 9.1±1.3 ppm, representing 14% variation from the average of the four samples. From these results, one can infer good

reproducibility of the nitrogen concentration. However, 43% variation in hydrogen concentration [H] was found at N/C=40,000 ppm in gas ratio ([H]=22.6±9.9 ppm) and 13% variation at N/C=20,000 ppm in gas ratio ([H]=12.5±1.6 ppm). Variation of the hydrogen concentration under the same growth parameters (or the same growth conditions) should be investigated using various methods in future studies.

As discussed above, the concentration of NVH centers in the negative or neutral charge state was found to be less than 10% of the total hydrogen detected by SIMS, meaning that most of the hydrogen has a form other than as a NVH center. Other forms of hydrogen incorporation include carbon dangling bond defects with hydrogen atoms. This defect was reportedly formed in CVD diamond film at concentrations of 0.4–28 ppm.[36] The concentration of this defect increased concomitantly with increasing amounts of non-radiative centers. However, the EPR signal corresponding to this defect was not detected from the samples examined in this study. Therefore, the form of hydrogen incorporated into the CVD diamond film has not been elucidated. The origin of this hydrogen is inferred to be either molecular hydrogen used as a carrier gas, or methane.

Reportedly, the CVD growth of diamond thin films while doping with boron and phosphorus leads to the incorporation of hydrogen.[37, 38, 39] In the case of boron, an equivalent amount of hydrogen is incorporated by forming B–H pairs. However, hydrogen incorporation mechanisms are not well studied for phosphorus or nitrogen. An absorption band at 3107 $cm^{-1}$ is proposed to be attributed to C–H bonds,[37] but this band was not observed in the samples examined for this study. Changing the carrier gas from hydrogen to deuterium might be effective at clarifying the mechanisms of hydrogen incorporation into the diamond film. Elucidation of the hydrogen incorporation mechanism is important for the further optimization of nitrogen-doped CVD diamond growth.

## Conclusion

For this study, we investigated CVD diamond crystals grown by nitrogen doping. The findings clarified the defect structures and charge states of nitrogen-related point defects in the crystals. The $^{15}N$-doped $^{12}C$-enriched free-standing homoepitaxial diamond (001) crystals were grown using microwave plasma chemical vapor deposition under oxygen-adding growth conditions. From results of various evaluations, the following findings were obtained. (1) Nitrogen is incorporated uniformly into the crystal. In fact, the standard deviation is less than 10% of the concentration. (2) Most of the nitrogen is isolated substitutional nitrogen. (3) Hydrogen is incorporated into the crystal in approximately the same amount as nitrogen. (4) About 10% of the nitrogen is in the form of an $NV^-$ center with hydrogen ($NVH^-$ center). (5) Both the NVH center and NV center are mostly negatively charged. The nitrogen concentration in the diamond crystal was controlled by changing the N/C gas ratio in the wide doping range of 10 ppb to 10 ppm.

An important finding is that 20–30% of the nitrogen-related defects are $N_s^+$ with lost electrons, meaning that some acceptors have density equivalent to the density of $N_s^+$. Understanding and reducing defects that act as acceptors is necessary for the formation of high-density $NV^-$ centers and for the resulting increase in magnetic sensitivity. We hope that various researchers will address the issues left as questions in this paper and that their important findings will be presented in future reports.

**Acknowledgments**

FTIR and PL measurements were performed by Ms. Shoko Manako of NIMS. This work was partially supported by MEXT Q-LEAP (JPMXS0118068379), JST CREST (JPMJCR1773), JST Moonshot R&D (JPMJMS2062), MIC R&D for construction of a global quantum cryptography network (JPMI00316), and JSPS KAKENHI (No. 20H02187 and 20H05661).

## References


[1] J.F. Barry, J.M. Schloss, E. Bauch, M.J. Turner, C.A. Hart, L.M. Pham, and R.L. Walsworth, Rev. Mod. Phys. **92**(1) (2020) 015004.

[2] T. Wolf, P. Neumann, K. Nakamura, H. Sumiya, T. Ohshima, J. Isoya, and J. Wrachtrup, Subpicotesla, Phys. Rev. X **5**(4) (2015) 041001.

[3] J.F. Barry, M.J. Turner, J.M. Schloss, D.R. Glenn, Y. Song, M.D. Lukin, H. Park, and R.L. Walsworth, P. Natl. Acad. Sci. USA **113**(49) (2016) 14133-14138.

[4] K. Arai, A. Kuwahata, D. Nishitani, I. Fujisaki, R. Matsuki, Y. Nishio, Z. Xin, X. Cao, Y. Hatano, S. Onoda, C. Shinei, M. Miyakawa, T. Taniguchi, M. Yamazaki, T. Teraji, T. Ohshima, M. Hatano, M. Sekino, and T. Iwasaki, Commun. Phys.– UK **5**(1) (2022) 200.

[5] C. Zhang, F. Shagieva, M. Widmann, M. Kubler, V. Vorobyov, P. Kapitanova, E. Nenasheva, R. Corkill, O. Rhrle, K. Nakamura, H. Sumiya, S. Onoda, J. Isoya, and J. Wrachtrup, Phys. Rev. Appl. **15**(6) (2021) 064075.

[6] C. Shinei, M. Miyakawa, S. Ishii, S. Saiki, S. Onoda, T. Taniguchi, T. Ohshima, and T. Teraji, Appl. Phys. Lett. **119**(25) (2021) 254001.

[7] N. Mizuochi, P. Neumann, F. Rempp, J. Beck, J. Jacques, P. Siyushev, K. Nakamura, D. J. Twitchen, H. Watanabe, S. Yamasaki, F. Jelezko, and J. Wrachtrup, Phys. Rev. B **80**, 041201(R) (2009) 041201.

[8] M. Miyakawa, C. Shinei, and T. Taniguchi, Jap. J. Appl. Phys. **61**(4) (2022) 045507.

[9] T. Teraji, High-quality and high-purity homoepitaxial diamond (100) film growth under high oxygen concentration condition, J. Appl. Phys. **118**(11) (2015) 115304.

[10] T. Teraji, T. Yamamoto, K. Watanabe, Y. Koide, J. Isoya, S. Onoda, T. Ohshima, L.J. Rogers, F. Jelezko, P. Neumann, J. Wrachtrup, and S. Koizumi, Phys. Status. Solidi. A **212**(11) (2015) 2365-2384.

[11] T. Teraji, Thin Solid Films **557** (2014) 231-236.

[12] C.S. Yan, Y.K. Vohra, H.K. Mao, and R.J. Hemley, P. Natl. Acad. Sci. USA **99**(20) (2002) 12523-12525.

[13] A. Chayahara, Y. Mokuno, Y. Horino, Y. Takasu, H. Kato, H. Yoshikawa, and N. Fujimori, Diam. Relat. Mater. **13**(11-12) (2004) 1954-1958.

[14] A. Tallaire, A.T. Collins, D. Charles, J. Achard, R. Sussmann, A. Gicquel, M.E. Newton, A.M. Edmonds, and R.J. Cruddace, Diam. Relat. Mater. **15**(10) (2006) 1700-1707.

[15] H. Watanabe, T. Kitamura, S. Nakashima, and S. Shikata, J. Appl. Phys. **105**(9) (2009).

[16] A. Tallaire, L. Mayer, O. Brinza, M.A. Pinault-Thaury, T. Debuisschert, and J. Achard, Appl. Phys. Lett. **111**(14) (2017).

[17] M.A. Lobaev, A.M. Gorbachev, S.A. Bogdanov, A.L. Vikharev, D.B. Radishev, V.A. Isaev, V.V. Chernov, and M.N. Drozdov, Diam. Relat. Mater. **72**(2017) 1-6.

[18] F. Omnes, P. Muret, P.N. Volpe, M. Wade, J. Pernot, and F. Jomard, Diam. Relat. Mater. **20**(7) (2011) 912-916.

[19] J. Lu, Y. Gu, T.A. Grotjohn, T. Schuelke, and J. Asmussen, Diam. Relat. Mater. **37**(2013) 17-28.

[20] Y. Mokuno, Y. Kato, N. Tsubouchi, A. Chayahara, H. Yamada, and S. Shikata, Appl. Phys. Lett. **104**(25) (2014) 252109.

[21] A. Tallaire, O. Brinza, P. Huillery, T. Delord, C. Pellet-Mary, R. Staacke, B. Abel, S. Pezzagna, J. Meijer, N. Touati, L. Binet, A. Ferrier, P. Goldner, G. Hetet, and J. Achard, Carbon **170**(2020) 421-429.

[22] T. Teraji, J. Isoya, K. Watanabe, S. Koizumi, and Koide, Mat. Sci. Sem. Proc. **70**(2017) 197-202.

[23] M. N. R. Ashfold, J. P. Goss, B. L. Green, P. W. May, M. E. Newton, and C. V. Peaker, Chemical Reviews **120** (12) (2020) 5745-5794.

[24] Y. Mokuno, A. Chayahara, H. Yamada, N. Tsubouchi, Diam. Relat. Mater. **18**(10) (2009) 1258-1261.

[25] A.M. Zaitsev, N.M. Kazuchits, K.S. Moe, J.E. Butler, O.V. Korolik, M.S. Rusetsky, and V.N. Kazuchits, Diam. Relat. Mater. **113** (2021) 108255.

[26] C. Shinei, Y. Masuyama, M. Miyakawa, H. Abe, S. Ishii, S. Saiki, S. Onoda, T. Taniguchi, T. Ohshima, and T. Teraji, J. Appl. Phys. **132**(21) (2022).

[27] A.M. Edmonds, U.F.S. D'Haenens-Johansson, R.J. Cruddace, M.E. Newton, K.M.C. Fu, C. Santori, R.G. Beausoleil, D.J. Twitchen, and M.L. Markham, Phys. Rev. B **86**(3) (2012) 035201.

[28] P. Deák, B. Aradi, M. Kaviani, T. Frauenheim, and A. Gali, Phys. Rev. B **89**(7) (2014) 075203.

[29] C.B. Hartland Ph.D. thesis, University of Warwick, Coventry, UK, (2014).

[30] S.C. Lawson, D. Fisher, D.C. Hunt, and M.E. Newton, J. Phys. – Condens. Mat. **10**(27) (1998) 6171-6180.

[31] A.T. Collins and G.S. Woods, Philos. Mag. B **46**(1) (1982) 77-83.

[32] R.U.A. Khan, P.M. Martineau, B.L. Cann, M.E. Newton, and D.J. Twitchen, J. Phys. – Condens. Mat. **21**(36) (2009) 364214.

[33] S. Liggins, M.E. Newton, J.P. Goss, P.R. Briddon, and D. Fisher, Phys. Rev. B **81**(8) (2010) 085214.

[34] L. Rondin, G. Dantelle, A. Slablab, F. Grosshans, F. Treussart, P. Bergonzo, S. Perruchas, T. Gacoin, M. Chaigneau, H.C. Chang, V. Jacques, and J.F. Roch, Phys. Rev. B **82**(11) (2010) 115449.

[35] T. Luo, L. Lindner, J. Langer, V. Cimalla, X. Vidal, F. Hahl, C. Schreyvogel, S. Onoda, S. Ishii, T. Ohshima, D. Wang, D.A. Simpson, B.C. Johnson, M. Capelli, R. Blinder, J. Jeske, New J. Phys. **24**(3) (2022) 033030.

[36] N. Mizuochi, H. Watanabe, H. Okushi, S. Yamasaki, J. Niitsuma, and T. Sekiguchi, Appl. Phys. Lett. **88**(9) (2006).

[37] J. Chevallier, A. Lusson, D. Ballutaud, B. Theys, F. Jomard, A. Deneuville, M. Bernard, E. Gheeraert, and E. Bustarret, Diam. Relat. Mater. **10**(3-7) (2001) 399-404.

[38] J. Chevallier, F. Jomard, Z. Teukam, S. Koizumi, H. Kanda, Y. Sato, A. Deneuville, and M. Bernard, Diam. Relat. Mater. **11**(8) (2002) 1566-1571.

[39] J.P. Goss, R. Jones, M.I. Heggie, C.P. Ewels, P.R. Briddon, and S. Oberg, Phys. Rev. B **65**(11) (2002).

>

## Figure captions

Figure 1 Optical microscope images of homoepitaxial diamond crystals. Brightfield reflection images of sample 1 (a) in an as-grown state and (b) after removal from the substrate. (c) Birefringence image of sample 1 after removal from the substrate. Brightfield reflection images of (d) sample 2 and (e) sample 3 after removal from the substrate.

Figure 2 Nitrogen, hydrogen, and boron depth profiles of (a) sample 1, (b) sample 2, (c) sample 3, (d) sample 4, and (e) sample 5. Silicon depth profiles are also shown for samples 4 and 5. (f) $^{12}C$ and $^{13}C$ depth profiles of sample 6.

Figure 3 EPR spectra of (a) sample 1, (b) sample 2, and (c) sample 3. Signals corresponding to the P1 center and $^{15}NVH$ center are shown.

Figure 4 FTIR absorption spectra corresponding to (a)–(c) $N_s^0$, (d)–(f) $N_s^+$, and (g)–(h) $NVH^0$ centers. The FTIR spectra of sample 1 are (a), (d), and (g), those of sample 2 are (b), (e), and (h), and those of sample 3 are (c), (f), and (i).

Figure 5 (a) PL spectra of samples 1–3. (b) Zero-phone line of the $NV^-$ and $NV^0$ centers of samples 1–3.

Figure 6 Abundance ratios of nitrogen-related defects of samples 1–3.

Figure 7 (a) Nitrogen concentrations as estimated by SIMS (red circles) and (blue triangles) as measured by EPR, as a function of the N/C gas ratio. (b) Hydrogen concentrations (green diamonds) estimated using SIMS as a function of the N/C gas ratio, along with the nitrogen concentration.